



# Reaction losses of charged particles in CsI(Tl) crystals

S. Sweany<sup>a,b</sup>, W.G. Lynch<sup>a,b,\*</sup>, K. Brown<sup>a</sup>, A. Anthony<sup>a,b</sup>, Z. Chajecski<sup>c</sup>, D. Dell'Aquila<sup>a,f,g</sup>,  
P. Morfouace<sup>d,e</sup>, F.C.E. Teh<sup>a,b</sup>, C.Y. Tsang<sup>a,b</sup>, M.B. Tsang<sup>a,b</sup>, R.S. Wang<sup>a</sup>, K. Zhu<sup>a,b</sup>

<sup>a</sup> National Superconducting Cyclotron Laboratory, Michigan State University, East Lansing, MI 48824, USA

<sup>b</sup> Department of Physics and Astronomy, Michigan State University, East Lansing, MI, 48824, USA

<sup>c</sup> Department of Physics and Astronomy, Western Michigan University, Kalamazoo, MI, 49008, USA

<sup>d</sup> CEA, DAM, DIF, F-91297 Arpajon, France

<sup>e</sup> Université Paris-Saclay, CEA, Laboratoire Matière en Conditions Extrêmes, 91680 Bruyères-le-Châtel, France

<sup>f</sup> Dipartimento di Chimica e Farmacia, Università degli Studi di Sassari, Sassari, Italy

<sup>g</sup> INFN-Laboratori Nazionali del Sud, Catania, Italy

## ARTICLE INFO

MSC:

00-01

99-00

Keywords:

Charged particle detector

Nuclear reaction losses

Multiple scattering

Detection efficiency

## ABSTRACT

To efficiently detect energetic light charged particles, it is common to use arrays of energy-loss telescopes involving two or more layers of detection media. As the energy of the particles increases, thicker layers are usually needed. However, carrying out measurements with thick-telescopes may require corrections for the losses due to nuclear reactions induced by the incident particles on nuclei within the detector and for the scattering of incident particles out of the detector, without depositing their full energy in the active material. In this paper, we develop a method for measuring such corrections and determine the reaction and out-scattering losses for data measured with the silicon-CsI(Tl) telescopes of the newly developed HiRA10 array. The extracted efficiencies are in good agreement with model predictions using the GEANT4 reaction loss algorithm for  $Z = 1$  and  $Z = 2$  isotopes. After correcting for the HiRA10 geometry, we obtain a general function that describes the loss of efficiency due to reaction losses in CsI(Tl) crystals as a function of range.

## 1. Introduction

Energy loss telescopes are often the tool of choice for detecting light charged particles and intermediate mass fragments emitted in nuclear collisions. At low energies, the detection material is frequently silicon. At intermediate energies above 10 MeV/A, a telescope more often consists of a Si detector backed by a thick scintillation detector. Thallium doped Cesium Iodide crystals (CsI(Tl)) are often selected to be this last scintillation detector. CsI(Tl) crystals have excellent energy resolution, are easily machinable, not especially hygroscopic, and produce light at wavelengths that match well with the response of silicon based photo-diodes [1,2]. They are also relatively inexpensive, allowing large arrays to be built.

The thicknesses of such scintillators are set by the range of the most penetrating particle to be measured. As the particle energy increases, the required thickness of such scintillators increases, and the likelihood that the incident particle will suffer a nuclear interaction within the scintillator also increases. In such cases, one observes events in which the incident particle only deposits a fraction of the expected electronic energy loss in the scintillator, reducing the electronic signal from the scintillator to a fraction of its normal value. The correlation between the energy loss “dE” in the first detector and the energy “E” in the last

detector for this particle becomes distorted, misplaced from the characteristic Particle IDentification (PID) line corresponding to that particle. For illustration, we use the HiRA10 Si-CsI array that is described in the next section. However, the reaction loss function derived at the conclusion of this paper is independent of detector geometry, allowing for the easy estimation of reaction loss probabilities.

Fig. 1 shows a typical HiRA10 PID plot that displays the characteristic PID lines for protons ( $p$ ), deuterons ( $d$ ) and tritons ( $t$ ) appearing as hyperbolic curves. Here, heliums ( ${}^3,4\text{He}$ ) lie slightly outside the boundaries of the figure. An intensity scale is provided at the right of the figure. Particles that suffer reaction losses or are scattered out of the crystal appear in the lower intensity haze to the left of the PID lines. Outscattering losses due to the Coulomb interaction can be large for protons in narrow CsI(Tl) crystals but they decrease when the area of the crystals is increased or if one excludes protons with trajectories parallel and adjacent to the sides of the detectors [3]. They also decrease with the mass for hydrogen isotopes and are rather small for helium isotopes. For all cases, nuclear reactions are more important than outscattering and are the major reason why the well identified isotopic yields are reduced; they provide the main source of uncertainty in the corrected isotopic spectra.

\* Department of Physics and Astronomy, Michigan State University, East Lansing, MI, 48824, USA.

E-mail address: [lynch@nscl.msu.edu](mailto:lynch@nscl.msu.edu) (W.G. Lynch).

The purpose of this work is to use experimental data obtained with the HiRA10 dE-E telescopes [4] to determine the reaction losses and check the reaction loss models studied in the work of Morfouace et al. [3]. If any Geant4 simulation, such as Morfouace et al. [3], reproduces the observed reaction loss effects, one can correct data for these reaction loss effects and assign a systematic error for the corrections.

To simplify analyses, it might be conceptually easier to study the reaction losses with a dedicated set of measurements wherein beams of identified particles with well-known energies are injected into the experimental detectors. That, however, would have required an extensive reconfiguration of our experimental setup, a significant amount of beam time and a separate experiment at another facility. In this paper, we demonstrate an alternate method that does not require such dedicated measurements. Instead, we check the accuracy of our reaction loss calculations and correct them as needed, using data from an experiment that is focused on the physics for which these reactions loss corrections are needed.

To apply this approach we employ Geant4 simulations with reasonable descriptions of the reaction cross sections for the incident particle on the nuclei that comprise the detector. Specifically, we performed Geant4 simulations within the NPTool framework [5], which provides a convenient coupling of GEANT4 version 10.01 to the ROOT analysis framework. These calculations, discussed in the simulations section, simulated the spectra for protons, deuterons, tritons,  $^3\text{He}$ , and alpha-particles in the HiRA10 detectors. Using the simulated and the experimental data, we expand upon methods developed by Avdeichikov et al. and Siwek et al. [6,7] to extract the reaction losses in the CsI(Tl) crystals of the HiRA10 charged particle data and compare them to the parameterizations of Morfouace [3]. To the extent that our GEANT4 simulations can successfully reproduce the observed reaction loss effects, we can correct the data and assign a systematic error for these corrections.

This requires an accurate algorithm for calculating the nuclear reaction cross section of that particle on Cesium and Iodine nuclei up to the maximum energy that can be stopped in the CsI(Tl) crystal. To calculate corrections that could be produced by GEANT4 users, Morfouace evaluated several global reaction cross section parameterizations that are implemented in GEANT4 [3]. He then showed that the Glauber model parameterization of Grishine for the proton reaction cross sections [8] provides a good description to both the proton total reaction cross sections on  $^{124}\text{Sn}$  targets and the angular distribution for scattered protons [3]. The global parameterization of Shen [9] was shown by Morfouace [3] to reproduce the measured  $^4\text{He}$  reaction cross sections on  $^{124}\text{Sn}$ , as well as the reaction cross sections obtained from optical model analyses of Ref. [10].

The 10 cm long HiRA10 CsI(Tl) crystals can measure protons up to 196 MeV. Therefore, Morfouace [3] required these algorithms to reproduce the systematics of high energy reaction cross sections, determined by beam attenuation methods in addition to reaction cross sections computed from optical model analyses of lower energy elastic scattering data. In addition, Morfouace [3] checked the accuracy of the simulated angular distribution of single scattering events to verify that the GEANT4 simulations will accurately calculate the loss due to multiple scattering in the crystal. At  $E/A \leq 40$  MeV, where there are many optical model calculations of elastic scattering, reaction losses were determined by Charity et al. [11] from optical model analyses. Their reported reaction losses for protons and tritons at  $E/A=40$  MeV are consistent with those of Morfouace et al. [3].

In the following section, we discuss the HiRA10 detector array used in this study. Section 3 delves into the methods developed for extracting the reaction losses through the comparison of simulated and experimental data. In Section 4 we present our conclusions.

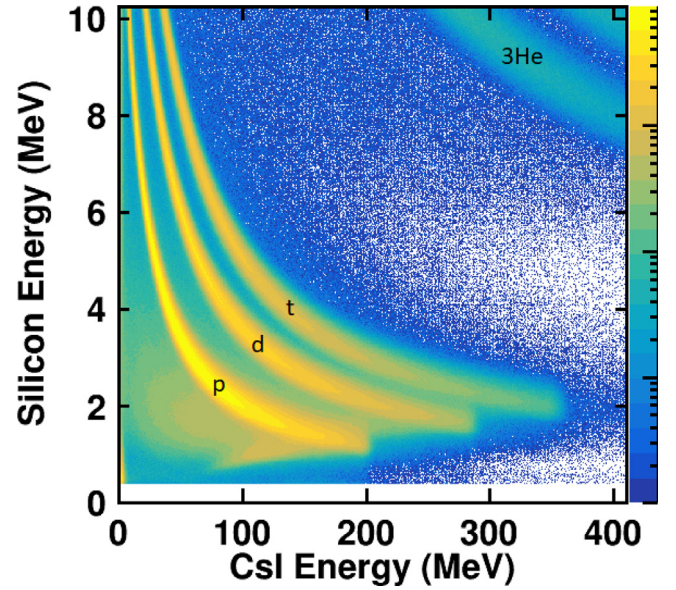


Fig. 1. Going from left to right the PID lines shown are protons, deuterons and tritons. The background haze to the left of the lines comes from reaction loss and out-scattering events.

## 2. HiRA10

The data for this study were collected using the HiRA10 Array, which consists of 12 dE-E charged-particle telescopes. Depending on the needs of a given experiment, the telescopes can be configured into different geometries. In the present experiment, the 12 telescopes were arranged into 3 towers with 4 telescopes in each tower. The telescopes cover a large range of polar angles. While the reactions of incident particles in each telescope are fundamentally the same, the relative intensities and energies of particle species varied throughout the array and differed for different projectile energies.

The first component of each HiRA10 telescope in the array is a 1.5 mm Double-Sided silicon Strip Detector (DSSD). Each DSSD used in this experiment had 32 1.95 mm wide front and 32 1.95 mm wide back strips oriented perpendicular to each other, allowing for the position where a particle enters the detector to be determined. The silicon detectors used in the HiRA10 Array are identical in design to those used in its predecessor, the High Resolution Array (HiRA) [12]. Backing the DSSD is a pack of four 10 cm long CsI(Tl) crystals supplied by Scionix in the Netherlands. Each crystal was cut so that they taper from the front of the telescope, (35x35 mm) to the back (44.6x44.6 mm). The front and back faces of the crystals are polished to a machined finish while the sides were sanded with 240 grit sand paper along the axis running perpendicular to the entrance window. The uniformly diffuse reflecting surface provided by sanding the sides of the crystals is important to achieving a position independent light output throughout each crystal [1]. A plastic light guide was attached to the back of each crystal using GE Bayer RTV615 silicon rubber glue. A 28x28 mm<sup>2</sup> Hamamatsu S3584-08 photo diode was attached to the back of the light guide using the same RTV615 glue. Each crystal was wrapped using a proprietary wrapping method developed by Scionix, wherein the sides were wrapped with a diffuse reflecting foil and the entrance window of the crystal was covered with a layer of 0.29 mg/cm<sup>2</sup> double-sided aluminized mylar foil. The light output uniformity of each crystals is determined by scanning it with an  $^{241}\text{Am}$  alpha source collimated to a spot size of 3 mm over a 3x3 grid [13]. The light output of each crystal did not vary by more than 1% for the 9 points measured during each scan. Details on the testing and performance of the silicon detectors can be found in [12,14]. We show a mechanical drawing of a single telescope in Fig. 2.

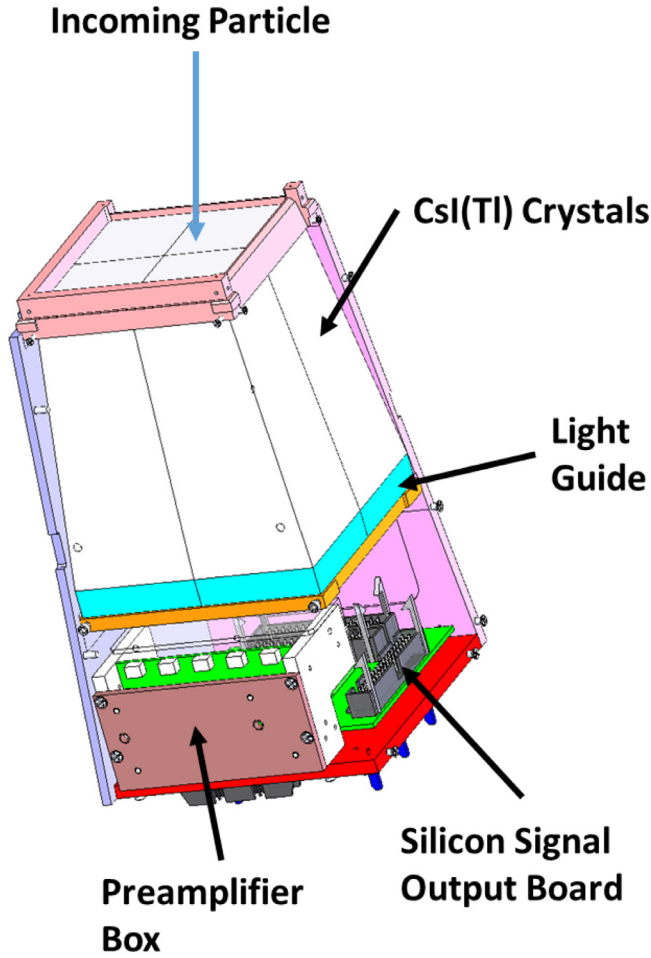


Fig. 2. HiRA10 Telescope mechanical drawing is shown with the silicon detector and two aluminum side panels removed. Four CsI(Tl) crystals and their four light guides can be seen in the figure. Also shown are the preamps for the CsI(Tl) signals and two connectors used to transmit the signals out of the aluminum box that encloses the telescope.

Charged particle data were measured with the HiRA10 array during a recent experimental campaign at the National Superconducting Cyclotron Laboratory in East Lansing, Michigan, using the Coupled Cyclotron Facility. Here we present data for three different reactions:  $^{48}\text{Ca} + ^{124}\text{Sn}$ ,  $^{40}\text{Ca} + ^{112}\text{Sn}$ , and  $^{48}\text{Ca} + ^{64}\text{Ni}$  that were measured at beam energies of  $E/A = 140$  MeV. For this analysis, data from two of the telescopes within the middle tower were used. These telescopes had data of reasonably high statistical precision, yet included only a limited amount of punch-through events as compared to the most forward angle telescopes where punch-through events were more prevalent.

### 3. CsI reaction loss analysis

Our reaction loss analysis proceeds as follows. First, we set a gate on position in the silicon detector to remove events in which particles are injected within 2 mm near the edge of a crystal and are more likely to be scattered out of the crystal due to Coulomb scattering by the Cesium (Cs) or Iodine(I) nuclei in the detector. Applying this gate, we performed Geant4 simulations to create events with and without nuclear reactions between the incident light particles and the Cs or I nuclei in the crystals. We impose gates on the energy deposited in the silicon dE on both the simulated and measured experimental events. We then separate the simulated events into (1) good (non-reacted) events where the incident particles lose their full incident energy in the telescope by electronic stopping and (2) (reacted) events

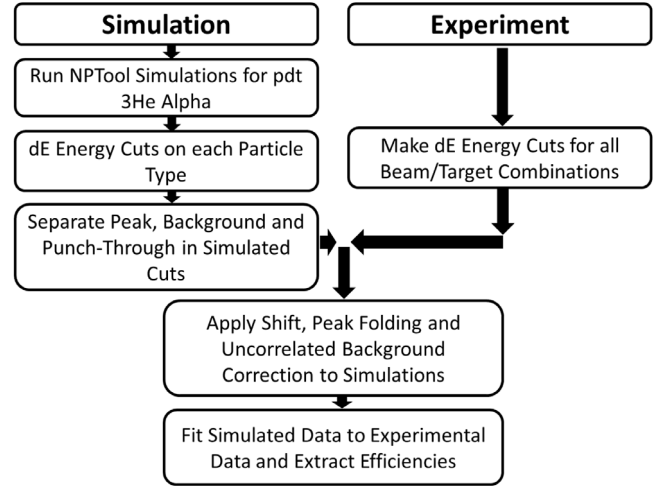


Fig. 3. Reaction Loss Analysis Flow Chart.

in which a reaction or out-scattering occurs. Next, corrections are made to the simulated data to account for small differences in the resolutions or calibrations of the experimental and simulated data. Finally, the simulated histograms are used to create fitting functions, which are then fitted to the corresponding dE cuts in the experimental data. Using these scaled histograms, the detection efficiency is then extracted for each of the light charged particle species. A flowchart describing the analysis method is shown in Fig. 3.

#### 3.1. Simulations

The first step of the reaction loss analysis is to simulate individual spectra for p, d, t,  $^3\text{He}$  and  $^4\text{He}$  with Geant4 simulations (version 10.04.02) using energy spectra similar to those of the corresponding particles in the experimental data. These GEANT4 simulations were performed using the NPTool framework. In these simulations, the standard Geant4 EMPhysicList Option4 was used to simulate electromagnetic scattering processes [5]. Different cross section parameterizations are available in GEANT4 to simulate the reactions in CsI(Tl) crystals for p, d, t,  $^3\text{He}$  and alpha particles. Following Ref. [3], we employ the Shen parameterization [9] to describe the reactions for d, t,  $^3\text{He}$  and alpha particles and the Grichine parameterization [8] for protons. We did not use Tripathi or the INCL parameterization since both produce reaction losses that are similar to the Shen parameterization [3].

While the detailed nuclear structure of the Cs and I nuclei is not fully modeled in the simulation, aspects of the  $\gamma$ -ray and particle decay de-excitation processes in central collisions are handled through GEANT4 with the G4DecayPhysics and G4RadioactiveDecayPhysics classes. The various decay particles, including  $\gamma$ -rays interact with CsI(Tl) as independent particles and their energy deposition in the crystal is summed with that of the incident light particle in calculating the signal in the CsI(Tl) crystal. For an inelastic collision wherein the projectile emits particles, the particle ID for the incident particle will be incorrect and will not be correctly calculated in the efficiency determination. However, the typical cross section for inelastic scattering leaving the nucleus in low-lying states is a few millibarns, whereas the total reaction cross section is of the order of a barn. This neglect of a detailed accounting for inelastic processes is small compared to the larger uncertainties we report below in the reaction cross section.

As expected, the number of charged particles lost due to reactions and out-scattering in the CsI(Tl) increases with the range of the particle, which is governed by its initial energy. Since the energy loss in the dE decreases inversely with energy, we can probe this range dependence by setting cuts on the dE. By selecting lower values of dE for a given



isotope, we select particles with higher incident energies and longer ranges and larger associated reaction losses. For each dE gate, we calculate CsI(Tl) spectra for the proton, deuteron, triton,  $^3\text{He}$  and alpha particles that are consistent with that gate. Since the dE value varies inversely with the E value for a given isotope, it is natural that the width of the dE cut must decrease with dE in order to make an effective selection on the incoming energy. Accordingly, we impose narrow dE cuts on the order of 25 KeV wide for  $dE < 1.5$  MeV, 50 KeV for  $1.5 \text{ MeV} < dE < 3.5$  MeV and 100 KeV for  $dE > 3.5$  MeV. Subject to these cuts on the energy loss in the silicon, dE, we create experimental and simulated spectra of the energies deposited in the CsI(Tl) detectors.

We classify the simulated CsI(Tl) events into non-reacted, reacted or punch-through events. (In the latter events, the particle penetrates fully through the CsI(Tl).) For each dE cut, three CsI(Tl) spectra are created for: (1) particles (p, d, t,  $^3\text{He}$  or alpha) that lose their total energy in the CsI(Tl) crystal, (2) particles that deposit part of their energy in the CsI(Tl) detector before reacting or scattering out of the detector, and (3) particles that traverse fully through the detector. The last group is referred to as “punch-through” particles, which are identified as events with an initial energy above the punch-through point. We label events as reaction loss/out-scattering events when they do not punch-through the CsI(Tl) detector but nevertheless still lose more than 1.5% of its initial energy. In between these two thresholds exists a 5–10 MeV region on either side of the punch-through point where range straggling can cause mixing between normal events, reaction loss events, out scattering events and punch-through events. For simplicity, we do not extract reaction losses using data in these regions where the mixing of processes is unclear. An example showing the separation between full energy deposition and reaction loss / out-scattering events at energies well below the “punch-through” energy is illustrated in Fig. 4 for a 100 KeV wide dE cut centered at 3.45 MeV. For this cut, the reaction loss contribution greatly exceeds the out-scattering contribution.

### 3.2. Corrections

Several corrections are made to the simulated data before they can be compared to the experimental data. The first is to shift the simulated data to match the peak positions in the experimental data. This is necessary because the nonlinear isotope dependence of the kinetic energy vs. light output relationship has to be taken into account in the simulation so that it matches the experimental spectra in Fig. 1. This is done by simply finding the position of relevant particle peaks (d, t,  $^3\text{He}$  and alphas) in both simulation and experimental data and dividing the position of the peaks to obtain a shift factor. This factor is then multiplied by the energy for each of the simulated reacted and non-reacted events, which shifts the simulated peaks and background to their appropriate locations in the PID spectrum.

At higher energies, corresponding to lower dE cuts, it becomes necessary to take punch-through events into account. The few deuteron and tritons with sufficient energy to punch through the detector contribute insignificantly in the current analysis. Proton punch through events, on the other hand, are more common and where they appear at high energies in the CsI(Tl) these punch-through events account for the majority of the background. For energies greater than 200 (198.5 to be exact) MeV, the proton punch-through tail folds over the proton PID line and trends towards lower energies in Fig. 1. We make some adjustments to match the calculated energy deposition for simulated punch-through events, to the measured ones.

Another problem with correcting for the punch-through is that we do not have information about the proton spectra above the punch through energy of 198.5 MeV. At such high energies, the precision of energy loss in the silicon detector is insufficiently precise to allow us to constrain the proton energy spectrum. We therefore assume for this region that reaction cross sections of the incident particles on the Cs or I nuclei do not change significantly at energies near and above 200 MeV.

To achieve accurate fits, we need to correct the line shape in the simulation to match that in the data. There are two issues: (1) the line

shape for one charged particle in the telescope is somewhat broader than the simulation and has a different shape at higher pulse heights that is not replicated by the simulation. (2) We can have coincidence summing of a charged particle hitting the crystal with a neutral particle that hits the same CsI(Tl) at the same time so that their signals in the CsI(Tl) overlap and add.

Regardless of the origin, the difference between the measured and calculated peak shape must be addressed. If the peak width of the simulations is narrower than that in the data, it will cause the fitting procedure to increase the background from reactions in order to fit the data near the peak, causing a nonphysical enhancement to the number of reacted particles. If the simulated peak width is wider than the data, it is also problematic because the fit will favor decreasing the number of reacted particles to better reproduce the data near the peak.

We have studied the distortions of the full energy peak due to the uncorrelated background. We find that much of the uncorrelated background in a dE-E detector results from the coincident summing involving one charged particle and one neutral particle. When more than one particle hits a given CsI(Tl) crystal, the resulting larger energy is incorrect and may push the particle outside its PID line.

At this point, it may be useful to clarify our terminology for “coincidence summing”. When two particles ionize the crystal so that electronic signals from their light emissions overlap, the output pulse is summed. When two particles are emitted from the target in the same event, or one is emitted from the target and the other is produced by the interaction of the first particle with nuclei in the detector, this can be labeled “true coincidence summing”. When they are from different events, this can be labeled as “random coincidence summing” or “pile-up”. In this experiment, the probability of pile-up is small, so we do not distinguish between random and true coincidence summing and just call it coincidence summing. If there were more pile-up events and they were confused with true coincidence summing of two particles emitted from the target, it would not matter for the purposes of this paper because we reject both pile-up and true coincidence events in the following analyses and the probability of such events is small.

Our analyses of the data compare the measured dE and E signals to the calculated dE and E signals from GEANT4 simulations for events with and without reactions. If a charged particle that has a nuclear reaction in the detector, the GEANT4 simulation sums the signal from the incident particle up to the reactions with the signals from reaction products emitted in the crystal from that nuclear reaction, and labels this event a nuclear reaction as discussed in the simulations section. To make legitimate comparisons, the GEANT4 subroutines model those decays and produce the expected light output including the light from the reaction products. As this is handled in the simulations and controlled by the reaction cross section routines, we focus on evaluating these reaction cross section routines for accuracy.

Coincident summing of two charged particles is suppressed in the experiment by the granularity of the silicon detector. Each CsI(Tl) crystal is covered by 256 pixels in the Si detector. Most of the events with two charged particles in a single CsI(Tl) hit different silicon strips and can thereby be identified and rejected so that the numbers of coincidence summing events involving two charged particles are correspondingly reduced.

We use the data to evaluate coincidence summing contributions. For example, we can correct for the uncorrelated background of a neutral particle in a CsI(Tl) crystal in coincidence with a charged particle that hits the silicon detector and that same CsI(Tl) crystal by using the data to identify similar events. For example, we look for events within a telescope where there is a good event (Silicon Hit + CsI Hit) and an uncorrelated event (CsI hit + No Silicon Hit) in the CsI(Tl) that is not adjacent to the first CsI(Tl) but rather lies diagonally across from it within the telescope can. To a good approximation, combining in software the latter events mimics the effect of a charged particle and a neutron or gamma both hitting the same CsI(Tl) crystal. All other combinations are similarly analyzed. This gives us an estimate of the

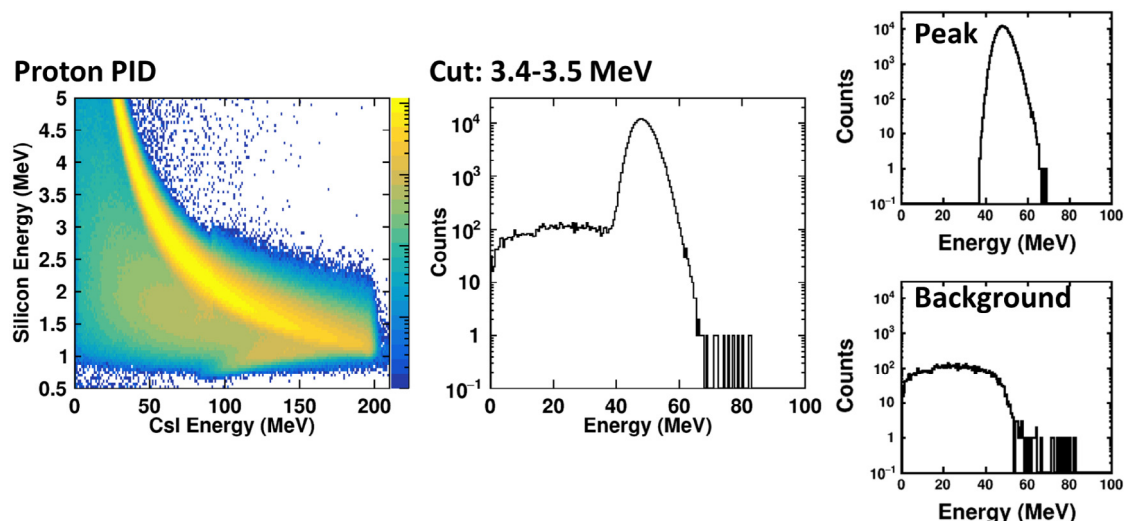


Fig. 4. Left: Simulated proton PID spectra. Middle: Example of a CsI(Tl) E spectrum for a dE cut from 3.4–3.5 MeV. Right: Simulated histograms after separation into “reacted” and “unreacted” protons: top shows protons, which deposited all of their energy and the bottom shows protons that did not deposit all of their energy due to either out-scattering or a reaction loss event.

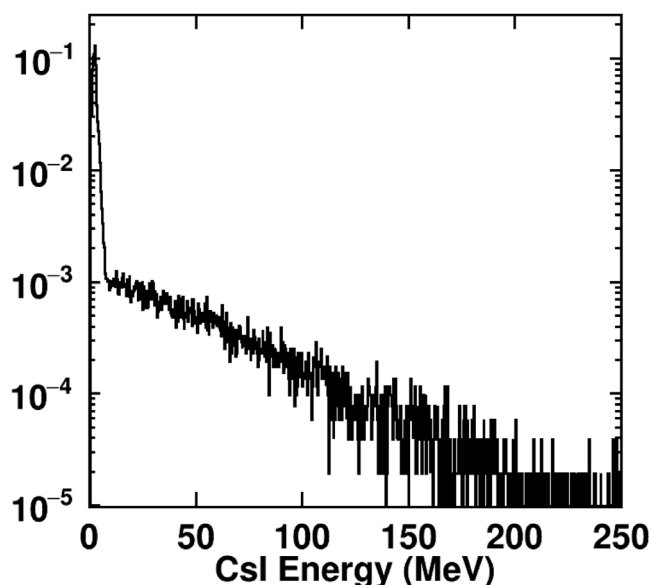


Fig. 5. Uncorrelated background energy distribution in the CsI normalized to 1.

fraction of the events that are affected by this form of uncorrelated background. After estimating what fraction of events are affected, we numerically combine the data from such events to calculate the coincidence summing signals and how this affects the spectrum.

Another example of coincidence summing concerns the case of a purely uncorrelated event where a low energy charged particle stops in the silicon while a neutral particle hits the CsI(Tl) behind it. The CsI(Tl) signal in such correlated background events is given by the neutral particle pulse height distribution. This is shown in Fig. 5 after employing the energy calibration to convert these pulse to their corresponding charged particle “energy” values. We use the CsI(Tl) energy distribution for uncorrelated background as a generating function to add a coincidence summing correction to the simulated data.

We find that the above cases account for about 80% of the uncorrelated events. To be complete, we performed additional studies to account for the situations where there were 2 and 3 uncorrelated particles in the crystal as well as corrections for the uncorrelated particles scattering between crystals.

The first example of coincidence summing of a charged particle and a neutral particle in the same CsI(Tl) turns out to be significant. While we find it does not strongly change the reaction loss values extracted for that charged particle, it does influence more strongly the reaction loss background for heavier particles. Consider those uncorrelated events that combine signals from neutral particles that react in a CsI(Tl) crystal with signals from protons, deuterons or tritons produced by reactions in the target and stop in the CsI(Tl) crystal but do not react with it. Such events contribute counts to the high energy (right) side of the p, d or t PID peaks. There they can be of the same order as reaction loss events involving the helium isotopes. If we do not make this coincidence summing correction, the reaction losses from  ${}^3\text{He}$  will be overestimated.

We now return to the small difference between the calculated and measured line shape for properly identified protons, deuterons, and tritons. The main effect here is a high energy tail on the CsI(Tl) spectrum that represents a few percent of the stopped events in the peak. The origin of this effect is not clear, but it does not reflect the intrinsic resolution of the CsI(Tl), which is of the order of 1%. It could reflect rare anomalous fluctuations in the dE energy loss signal caused by channeling or by variations in the thickness of the silicon detectors, for example. To correct the calculated line-shape, we randomly add “noise” according to a noise distribution to each simulated CsI(Tl) signal. This noise spectrum is calculated using a sum of “modified Gaussians” that are products of an exponential and the complementary error function

Following an approach similar to that of Ref. [15,16], We use a linear combination of three “modified Gaussians” with each having different exponential tails, but retaining the same standard deviation and mean. We adjust the tail parameters of these modified Gaussians to replicate the shape of the peak; two of the modified Gaussians have a tail on the right side of the peak and the third has a tail on the left side of the peak. We also adjust the probabilities for each of these functions to optimize the description of the peak. Fig. 6 shows protons within a dE cut from 3.4–3.5 MeV with the panels showing both the experimental data (open points) and simulated data (solid lines) with different corrections being applied. The upper left panel shows the differences between experimental and simulated line shapes with no correction. Adding coincidence summing corrections (upper right panel) changes the simulated line shape very little. The bottom left panel shows how the Gaussian smearing adjusts the high energy tail of the simulated spectrum to better approximate the data. Again, adding coincidence summing corrections (lower right panel) changes the overall line shape insignificantly.

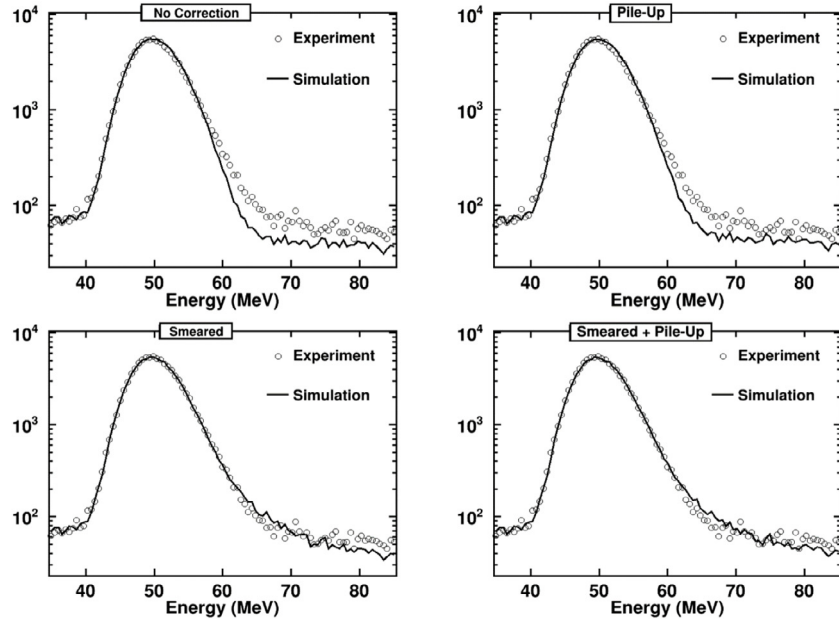


Fig. 6. The four panels show protons for a cut on dE from 3.4–3.5 MeV. Open points show the experimental data and the solid line shows the simulated protons with different corrections applied as follows for the different panels. Upper Left: No correction, Upper Right: Correction for uncorrelated background, Lower Left: Correction for Gaussian folding, Lower Right: Both corrections.

### 3.3. Fitting

After corrections are made to the calculated spectra for all of the simulated effects involving the reacted and non-reacted particles, these histograms are then fit to the observed spectra to determine the reaction losses in the crystals. This process is repeated for each of the individual dE cuts.

The calculated peak and background histograms for different light charged particle species are parameterized for fitting using Eq. (1) where  $P_i$  and  $B_i$  represent the peak and background histograms for particle  $i$  within a dE gate, respectively.  $A_i$  is an overall normalization constant that reflects the number of incident particles at an incident energy corresponding to the energy loss dE gate for particle  $i$ .  $A_i$  adjusts the overall magnitude of the simulated histograms. A second normalization constant,  $a_i$  (typically of order unity) is applied to the background histogram to account for differences in the predicted and observed reaction loss background. A value of  $a_i = 1$  would imply that the reaction loss corrections of Ref. [3], i.e. the Shen parameterization [9] to describe the reactions of d, t,  $^3\text{He}$ ,  $^4\text{He}$  in the CsI(Tl) and the Grichine parameterization [8] for protons, perfectly describe the data for these particles at the energies being calculated.

$$f(dE) = \sum_i A_i (P_i + a_i B_i) \quad (1)$$

To check the consistency of the reaction loss determination, cuts for  $^{48}\text{Ca} + ^{124}\text{Sn}$ ,  $^{40}\text{Ca} + ^{112}\text{Sn}$ , and  $^{48}\text{Ca} + ^{64}\text{Ni}$  were simultaneously fitted using the simulated data. By choosing three systems with different  $N/Z$  ratios, we gain sensitivity that helps us to constrain the reaction losses from the different isotopes. During fitting, the overall scaling parameter  $a_i$  for the different particle species was allowed to vary freely, reflecting the fact that the relative abundances of the heavier hydrogen and helium isotopes become larger as the projectile and target become more neutron rich. However, the same background scaling factor  $a_i$  is used for all systems, because it is proportional to the ratios of the measured/calculated reaction losses, which should be independent of the reaction. Thus, the simultaneous fitting of 3 systems allows the values for  $a_i$  to be better constrained, which is the main goal of this work. For higher energy hydrogen isotopes that penetrate the last 5 cm of the CsI crystal, we obtained average values for  $a_i$  of approximately 1.0 for protons, 1.24 for deuterons and 1.19 for tritons. For the helium

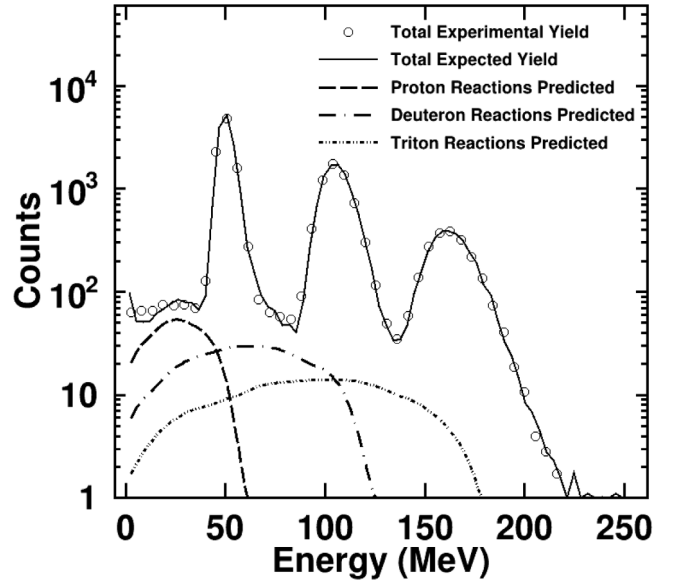


Fig. 7. Fit on a dE cut between 3.4 and 3.5 MeV for  $^{48}\text{Ca} + ^{124}\text{Sn}$ . Experimental data are shown as the open points while the overall fit using the simulated histograms is illustrated with the solid line. Fits to the background are shown for protons, deuterons and tritons and shown as dashed, dot-dashed and dotted lines.

isotopes, the average of best fit values for  $a_i$  remained close to 1.0 over the energy range we could measure.

Fig. 7 illustrates the quality of the reproduction of the measured data by the simulation for a dE cut centered on 3.45 MeV. Here we show the experimental yield as well as the simulated background spectra for protons, deuterons and tritons that react within the CsI(Tl) crystal. From the fits described above, reaction losses and resulting efficiencies for the five light particles are extracted by dividing the total number of counts in the scaled peak by the sum of the counts in the scaled peak plus background. While we are able to determine the reactions losses up to the punch through energies for Hydrogen isotopes in the HiRA10 crystals, efficiencies for  $^3\text{He}$  and alpha parties, could only

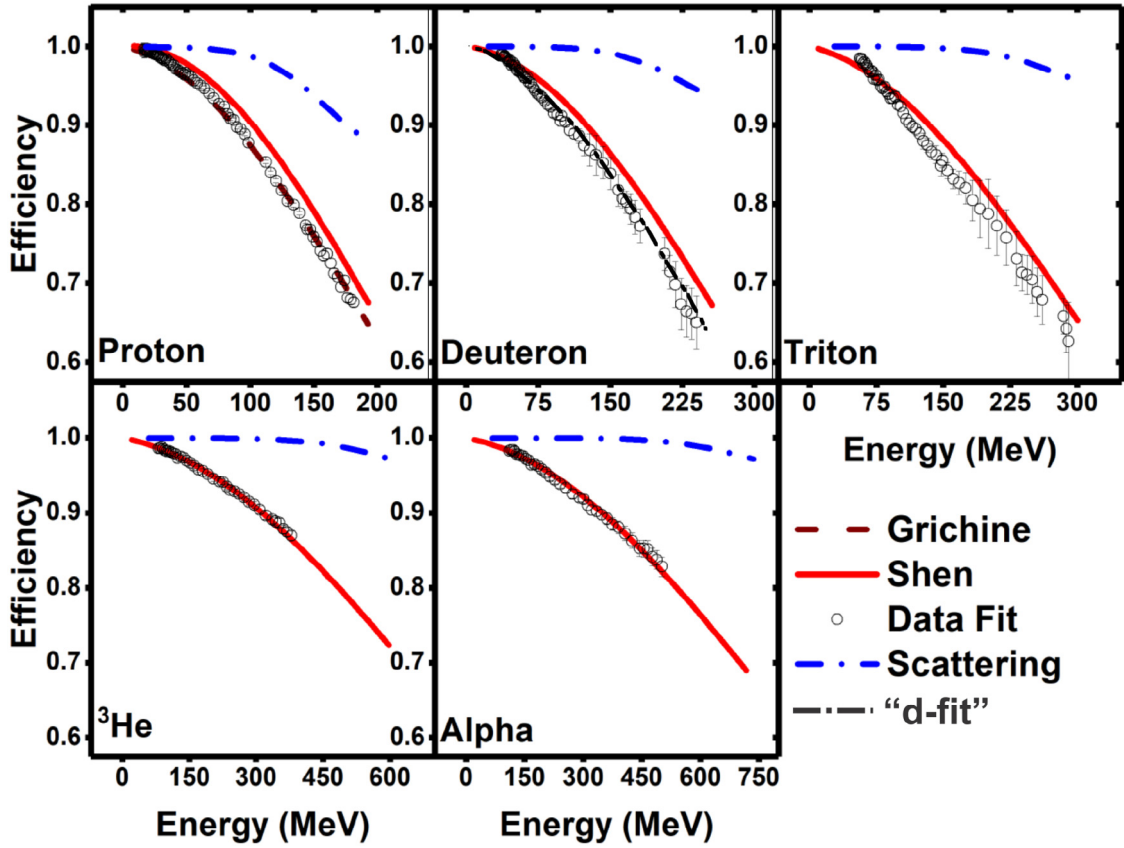


Fig. 8. Light charged particle efficiencies as a function of energy. Each panel shows the extracted efficiency (open points) as well as the simulated efficiency using the Shen cross section parameterization (solid lines) and the efficiency coming from only multiple scattering (dot dashed lines). For protons, we also include the efficiency using the Grichine parameterization (long dashed line), which describes the reaction losses better. For deuterons, we also include the efficiency using the “d-fit” parameterization (long dashed line), which describes the reaction losses better.

be extracted up to 375 and 500 MeV, respectively, due to the lack of statistics at higher energies.

Fig. 8 shows the efficiency values for our data. Error bars for the extracted efficiencies (data points) reflect both statistical errors as well as ambiguities in fit parameters from the scaled peak and background histograms. Such systematic uncertainties influence the uncertainties for deuterons and tritons most because the values extracted for their reaction loss contributions are somewhat anti-correlated, where an anomalously large value for the scaling parameter for the deuteron background was usually accompanied by an anomalously small value for the triton background and vice versa.

The extracted efficiencies in Fig. 8 reflect both reaction and out-scattering losses so the total loss is dependent on the geometry of the detector and any collimation that restricts the volume of the crystal used for detection. The largest out-scattering contributions (dot-dashed curves) occur for protons, due to its larger charge/mass ratio. They are on the order of 10% of the total losses at the highest energy (200 MeV). In this work, we require particles to pass through a region of the silicon detector that lies at least 2 mm from the edge of the CsI(Tl) crystal. That requirement was not imposed in Ref. [3]. Vetoing charged particles that pass through these outer silicon strips reduces the numbers of particles lost to out-scattering and the efficiencies in this work are somewhat larger than those in [3] but still within their stated 3% uncertainty for proton and He isotopes.

Since the measured and calculated reaction losses for  $^3\text{He}$  and  $^4\text{He}$  are in excellent agreement with the available data, it appears likely that the Shen parameterization describes the reaction losses accurately at energies beyond where we can confirm their accuracy. For protons, the Grichine parameterization (black dashed line) predictions agree with the data better than the Shen parameterization. The simulated

efficiencies for deuterons and tritons overestimate the measured values by about 5% at the punch-through point. It appears that the Shen cross sections adopted by Morfouace et al. [3] are smaller than what is needed to predict the reaction losses for deuterons and tritons correctly. Morfouace noted that the Shen reaction cross section underpredicts the available deuteron reaction cross section on  $^{124}\text{Sn}$  and therefore proposed an alternative deuteron cross section expression “d-fit”. The “d-fit” curve for the deuteron reaction cross section is also shown in Fig. 8 and is closer to the measured deuteron efficiency. Regardless of whether one uses the Shen or the “d-fit” reaction sections, all observed differences between calculated and measured efficiencies are small and systematic and can be addressed by a simple empirical correction of the order of a few percent.

Out-scattering primarily occurs for particles that enter the crystals near the crystal boundary. It becomes more prevalent for smaller crystals where a larger fraction of the incident particles can enter the crystal near the crystal boundary. Since GEANT4 does not allow calculations without Coulomb interactions, performing a “pure” reaction loss calculation is not an option. Out-scattering can be negligible for a highly collimated beam of particles that enters a very large crystal, providing one method to get the “pure” reaction loss efficiency. Because out-scattering depends on crystal geometry, it is interesting to know what the current measurements imply in the limit of negligible out-scattering. For our smaller crystals, one can approximate the corresponding values for the effect of pure reaction losses by renormalizing away the fraction that does not out-scatter (blue dot-dashed curves in Fig. 8). This effectively renormalizes the flux in the full calculations so that there is no loss in flux due to out-scattering.

So there are two approaches to calculate “pure” reaction loss efficiencies: (1) calculating it with a highly collimated beam and (2)



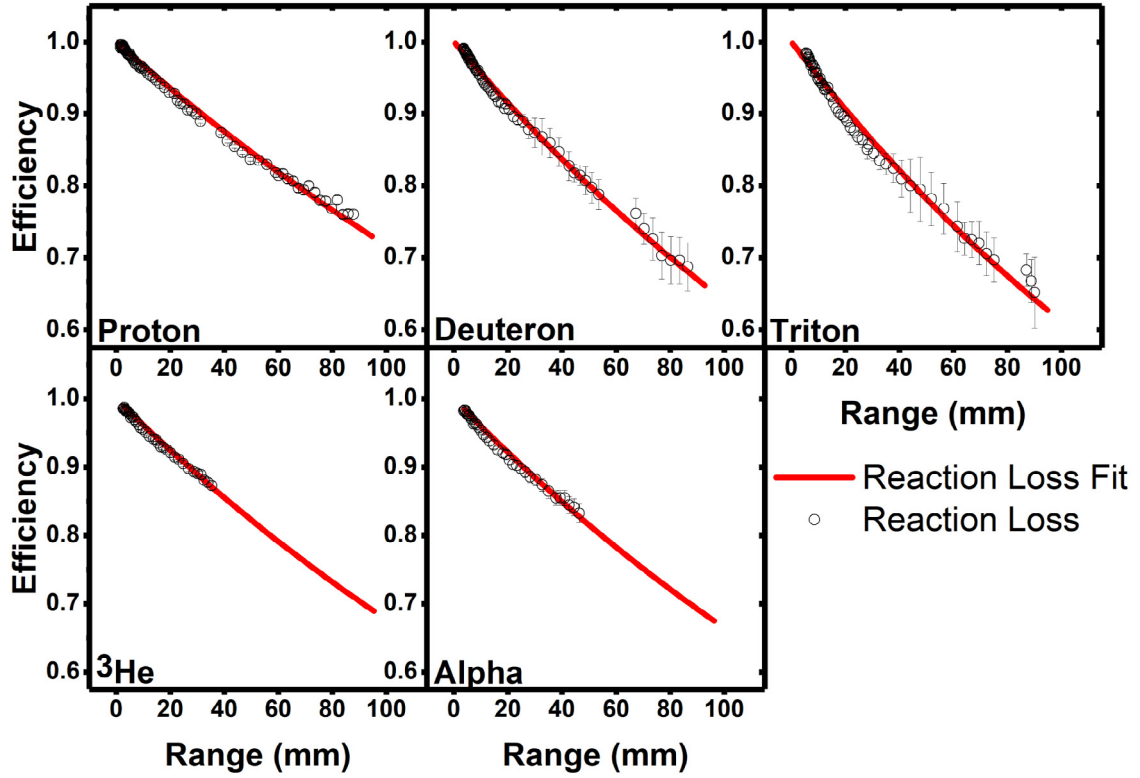


Fig. 9. Efficiency as a function of range for the five light charged particle species. The open points come from the fitted data with multiple scattering efficiency removed and the solid blue line is the fit of these points using Eq. (2). The fitting parameter values “ $c$ ” (in  $\text{mm}^{-1}$ ) are  $3.33 \times 10^{-3}$  for protons,  $4.45 \times 10^{-3}$  for deuterons,  $4.92 \times 10^{-3}$  for tritons,  $3.9 \times 10^{-3}$  for  $^3\text{He}$  and  $4.08 \times 10^{-3}$  for alphas.

dividing away the out-scattering efficiency. We have compared the two approaches for protons, which have the largest out-scattering corrections and find that the two approaches agree to better than 1%. This is useful because we can obtain pure reaction loss efficiencies by dividing the experimentally measured efficiency by the calculated out-scattering efficiency. This allows us to obtain “pure” reaction loss efficiencies for  $d$  and  $t$ , which GEANT4 does not currently reproduce.

The resulting “pure” reaction loss efficiency plotted as a function of range (the calculated depth of the detector that is penetrated by a particle) is shown in Fig. 9. The energy to range conversion is performed with LISE [17]. Here, we plot the pure efficiency as a function of range instead of energy, because the incident particle flux decreases exponentially with the thickness of the detection material traversed in the limit of a constant reaction cross section. For simplicity, we have fitted the “pure” reaction loss efficiency values in Fig. 9 with Eq. (2). This results in the fits shown as solid red lines. The fitting parameters “ $c$ ” in units of  $\text{mm}^{-1}$  are  $3.33 \times 10^{-3}$  for protons,  $4.45 \times 10^{-3}$  for deuterons,  $4.92 \times 10^{-3}$  for tritons,  $3.9 \times 10^{-3}$  for  $^3\text{He}$  and  $4.08 \times 10^{-3}$  for alphas. It is then straight forward to apply the efficiency correction to other detector systems. One simply multiplies the efficiency for multiple scattering generated by GEANT4 by the reaction loss efficiency from Eq. (2).

$$E_{\text{Reactions}}(R) = e^{-cR} \quad (2)$$

#### 4. Conclusions

Using a technique that can be applied to different energy loss telescopes, we have carefully tested the recent reaction loss modeling of Ref. [3] for Hydrogen and Helium isotopes in CsI(Tl) experimentally. We find that our measured proton reaction losses match well with the Grichine cross section parameterizations at high energies. Similarly,  $^3\text{He}$  and alphas also match very well with the Geant4 calculations with the Shen parameterization. On the other hand, both deuterons

and tritons have lower efficiencies than the Shen parameterization predictions by several percent, varying from low to high energies. This is consistent with the finding of Morfouace et al. [3] who found that all of the available GEANT4 parameterizations underestimated the reaction cross section for deuterons on CsI(Tl). The difference, however, is relatively small and, once realized, can be easily corrected after running simulations with the Shen parameterization. We have also derived a formula with best fit parameters for the reaction loss efficiency as a function of range for CsI(Tl) crystals. This formula can be applied to any detector system by providing the GEANT4 efficiencies from multiple scattering which is specific to an individual detector.

#### CRediT authorship contribution statement

**S. Sweany:** Writing, Conceptualization, Software, Data curation, Visualization, Formal analysis, Writing - review & editing, Investigation. **W.G. Lynch:** Supervision, Writing - review & editing, Conceptualization, Funding acquisition, Investigation. **K. Brown:** Supervision, Resources, Investigation. **A. Anthony:** Resources, Investigation. **Z. Chajekski:** Project administration, Investigation. **D. Dell’Aquila:** Conceptualization, Software, Investigation. **P. Morfouace:** Conceptualization. **F.C.E. Teh:** Validation, Investigation. **C.Y. Tsang:** Resources, Validation, Investigation. **M.B. Tsang:** Supervision, Writing - review & editing, Funding acquisition, Investigation. **R.S. Wang:** Software, Investigation, Validation, Software, Data curation. **K. Zhu:** Software, Investigation.

#### Declaration of competing interest

The authors declare that they have no known competing financial interests or personal relationships that could have appeared to influence the work reported in this paper.



## Acknowledgments

This work is supported by the U.S. National Science Foundation under Grants No. PHY-1565546 and PHY-1712832 and by the U.S. Department of Energy (Office of Science) under Grant No. DE-SC0014530, DE-SC0021235, DE-NA0002923, and DE-NA0003908. The authors would also like to thank the HiRA group.

## References

- [1] W. Gong, Y. Kim, G. Poggi, Z. Chen, C. Gelbke, W. Lynch, M. Maier, T. Murakami, M. Tsang, H. Xu, K. Kwiatkowski, Resolution tests of CsI(Tl) scintillators read out by pin diodes, *Nucl. Instrum. Methods Phys. Res. A* 268 (1) (1988) 190–199, [http://dx.doi.org/10.1016/0168-9002\(88\)90605-5](http://dx.doi.org/10.1016/0168-9002(88)90605-5), URL <http://www.sciencedirect.com/science/article/pii/0168900288906055>.
- [2] A. Wagner, W. Tan, K. Chalut, R. Charity, B. Davin, Y. Larochelle, M. Lennek, T. Liu, X. Liu, W. Lynch, A. Ramos, R. Shomin, L. Sobotka, R. [de Souza], M. Tsang, G. Verde, H. Xu, Energy resolution and energy–light response of CsI(Tl) scintillators for charged particle detection, *Nucl. Instrum. Methods Phys. Res. A* 456 (3) (2001) 290–299, [http://dx.doi.org/10.1016/S0168-9002\(00\)00542-8](http://dx.doi.org/10.1016/S0168-9002(00)00542-8), URL <http://www.sciencedirect.com/science/article/pii/S0168900200005428>.
- [3] P. Morfouace, W. Lynch, M. Tsang, Charged-particle detection efficiencies of close-packed CsI arrays, *Nucl. Instrum. Methods Phys. Res. A* 848 (2017) 45–53, <http://dx.doi.org/10.1016/j.nima.2016.12.045>, URL <http://www.sciencedirect.com/science/article/pii/S0168900216313122>.
- [4] D. Dell'Aquila, S. Sweany, K. Brown, Z. Chajecski, W. Lynch, F. Teh, C.-Y. Tsang, M. Tsang, K. Zhu, C. Anderson, A. Anthony, S. Barilini, J. Barney, A. Camaiani, G. Jhang, J. Crosby, J. Estee, M. Ghazali, F. Guan, O. Khanal, S. Kodali, I. Lombardo, J. Manfredi, L. Morelli, P. Morfouace, C. Niu, G. Verde, Non-linearity effects on the light-output calibration of light charged particles in CsI(Tl) scintillator crystals, *Nucl. Instrum. Methods Phys. Res. A* 929 (2019) 162–172, <http://dx.doi.org/10.1016/j.nima.2019.03.065>, URL <http://www.sciencedirect.com/science/article/pii/S0168900219303961>.
- [5] A. Matta, P. Morfouace, N. de Séréville, F. Flavigny, M. Labiche, R. Shearman, NPTool: a simulation and analysis framework for low-energy nuclear physics experiments, *J. Phys. G: Nucl. Part. Phys.* 43 (4) (2016) 045113, <http://dx.doi.org/10.1088/0954-3889/43/4/045113>.
- [6] V. Avdeichikov, A. Fomichev, B. Jakobsson, A. Rodin, G. Ter-Akopian, Reaction losses of light charged particles in CsI, BGO and GSO scintillators, *Nucl. Instrum. Methods Phys. Res. A* 437 (2) (1999) 424–431, [http://dx.doi.org/10.1016/S0168-9002\(99\)00774-3](http://dx.doi.org/10.1016/S0168-9002(99)00774-3), URL <http://www.sciencedirect.com/science/article/pii/S0168900299007743>.
- [7] A. Siwek, A. Budzanowski, B. Czech, A. Fomichev, T. Gburek, A. Rodin, I. Skwirczynska, R. Wolski, Incomplete energy deposition in long CsI(Tl) crystals, *Nukleonika* 47 (4) (2002) 141–145.
- [8] V. Grichine, A simplified Glauber model for hadron–nucleus cross sections, *Eur. Phys. J. C* 62 (2) (2009) 399–404.
- [9] W.-q. Shen, B. Wang, J. Feng, W.-l. Zhan, Y.-t. Zhu, E.-p. Feng, Total reaction cross section for heavy-ion collisions and its relation to the neutron excess degree of freedom, *Nuclear Phys. A* 491 (1989) 130–146, [http://dx.doi.org/10.1016/0375-9474\(89\)90209-1](http://dx.doi.org/10.1016/0375-9474(89)90209-1).
- [10] C. Perey, F. Perey, Compilation of phenomenological optical-model parameters 1954–1975, *At. Data Nucl. Data Tables* 17 (1) (1976) 1–101.
- [11] R. Charity, L. Sobotka, N. Robertson, D. Sarantites, J. Dinius, C. Gelbke, T. Glasmacher, D. Handzy, W. Hsi, M. Huang, W. Lynch, C. Montoya, G. Peaslee, C. Schwarz, M. Tsang, Prompt and sequential decay processes in the fragmentation of 40 MeV/nucleon  $^{20}\text{Ne}$  projectiles, *Phys. Rev. C* 52 (1995) 3126–3150, <http://dx.doi.org/10.1103/PhysRevC.52.3126>, URL <https://link.aps.org/doi/10.1103/PhysRevC.52.3126>.
- [12] M. Wallace, M. Famiano, M.-J. [van Goethem], A. Rogers, W. Lynch, J. Clifford, F. Delaunay, J. Lee, S. Labostov, M. Mocko, L. Morris, A. Moroni, B. Nett, D. Oostdyk, R. Krishnasamy, M. Tsang, R. [de Souza], S. Hudan, L. Sobotka, R. Charity, J. Elson, G. Engel, The high resolution array (HiRA) for rare isotope beam experiments, *Nucl. Instrum. Methods Phys. Res. A* 583 (2) (2007) 302–312, <http://dx.doi.org/10.1016/j.nima.2007.08.248>, URL <http://www.sciencedirect.com/science/article/pii/S016890020701947X>.
- [13] S.R. Sweany, Constraining Proton/Neutron Effective Mass Splitting through Heavy Ion Collisions (Ph.D. thesis), Michigan State University, 2020.
- [14] M.-J. [van Goethem], M. Wallace, B. Nett, M. Famiano, K. Herner, D. Oostdyk, M. Mocko, W. Lynch, M. Tsang, P. Schotanus, J. Telfer, H. Clark, A. Moroni, R. [de Souza], L. Sobotka, Investigations and corrections of the light output uniformity of CsI(Tl) crystals, *Nucl. Instrum. Methods Phys. Res. A* 526 (3) (2004) 455–476, <http://dx.doi.org/10.1016/j.nima.2004.02.038>, URL <http://www.sciencedirect.com/science/article/pii/S0168900204005388>.
- [15] G. Bortels, P. Collaers, Analytical function for fitting peaks in alpha-particle spectra from si detectors, *Int. J. Rad. Appl. Instrum. [A]* 38 (10) (1987) 831–837, [http://dx.doi.org/10.1016/0883-2889\(87\)90180-8](http://dx.doi.org/10.1016/0883-2889(87)90180-8), URL <http://www.sciencedirect.com/science/article/pii/0883288987901808>.
- [16] S. Pommé, B. Caro Marroyo, Improved peak shape fitting in alpha spectra, *Appl. Radiat. Isot.* 96 (2015) 148–153, <http://dx.doi.org/10.1016/j.apradiso.2014.11.023>, URL <http://www.sciencedirect.com/science/article/pii/S0969804314004175>.
- [17] D. Bazin, O. Tarasov, M. Lewitowicz, O. Sorlin, The program LISE: a simulation of fragment separators, *Nucl. Instrum. Methods Phys. Res. A* 482 (1) (2002) 307–327, [http://dx.doi.org/10.1016/S0168-9002\(01\)01504-2](http://dx.doi.org/10.1016/S0168-9002(01)01504-2), URL <https://www.sciencedirect.com/science/article/pii/S0168900201015042>.